Reduction of efficiency droop in c-plane InGaN/GaN light-emitting diodes using a thick single quantum well with doped barriers

Y C Chow, C. Lynsky, F. Wu, S. Nakamura, S P Denbaars, C. Weisbuch, J S Speck

Reduction of efficiency droop in *c*-plane InGaN/GaN light-emitting diodes using a thick single quantum well with doped barriers

Y. C. Chow[1,*], C. Lynsky[1], F. Wu[1], S. Nakamura[1,2], S. P. DenBaars[1,2], C. Weisbuch[1,3] and J. S. Speck[1]

[1] *Materials Department, University of California, Santa Barbara, CA 93106, USA*
[2] *Department of Electrical and Computer Engineering, University of California, Santa Barbara, CA 93106, USA*
[3] *Laboratoire de Physique de la Matière Condensée, CNRS, Ecole Polytechnique, IP Paris, 91128 Palaiseau, France*
** Electronic mail : yichao@ucsb.edu*

We report on *c*-plane InGaN/GaN single quantum well (QW) light-emitting diodes (LEDs) of different well widths (3 or 9 nm) with and without doped barriers. QW barriers were doped with the aim of reducing the internal electric field (F_{QW}) in the QW to increase the electron-hole overlap, therefore increasing the recombination rates and resulting in the reduction of the efficiency droop. We indeed observed, through biased photocurrent spectroscopy, a reduction in F_{QW} with doped barriers, with F_{QW} being in the same direction of the *p-n* junction field at zero bias as opposed to the junction field for LEDs without doped barriers. Even with the improvement of ground state wavefunction overlap, the ground state transition rate remains low for thick QWs. Transitions through excited states were observed for both thick QW LEDs with and without doped barriers. The thick QW LED without doped barriers displayed low external quantum efficiency (EQE), likely as a result of the carrier overflow due to the poor confinement of carriers in the excited states. On the other hand, for LED with doped barriers, the flatter band in the QW resulting from the lower F_{QW} reduces the energy separation between the eigenstates, leading to better confinement of carriers in the excited states. With doped barriers, we demonstrated a low efficiency droop 9-nm-thick single QW LED with a peak EQE of 42% at 40 A/cm^2 and an EQE of 36% at 400 A/cm^2.

One of the most enduring challenges faced by InGaN/GaN light-emitting diodes (LEDs) is the efficiency droop phenomenon, which refers to the decrease of the quantum efficiency with increasing injection current density. The origin of efficiency droop is still being debated, with proposed causes including Auger recombination and carrier leakage.[1–3] All these mechanisms dominate at high carrier densities (n) in the active region. A straightforward way to delay the onset of efficiency droop is by increasing the active region volume to lower n, where different approaches have been attempted in the past.[4–8] One such approach was to have LEDs with multiple-quantum-well (MQW) active regions, a method that was unsuccessful in mitigating the droop due to poor hole transport and non-uniform carrier distribution in the quantum wells (QWs). Recombination happens mainly in the QW closest to the p-GaN, rendering most of the QWs ineffective in reducing the impact of droop.[9,10] The approach of using a thick InGaN layer active region has shown some encouraging results in the past.[4–7] Another approach has shown that it is possible to reduce the internal electric field (F_{QW}) in the c-plane QWs through the use of doped barriers.[11–14]. The resulting improvement in wavefunction overlap increases both the nonradiative and radiative recombination rates[15,16] which lead to a decrease in n at a given current density, thereby delaying the efficiency droop onset.[12,17] Young *et al.* reported the complete screening of the polarization field in a c-plane single QW (SQW) as thick as 7.5 nm by placing heavily doped Mg(Si)-doped $p(n)$-type GaN barriers next to the QW.[12] The LEDs, however, suffered from high Shockley-Read-Hall (SRH) recombination as heavily doped layers are known to cause degradation of the epitaxial morphology and introduce nonradiative recombination centers (NRCs) in the LEDs. Despite these challenges, through growth optimization, it is possible to reduce the detrimental impact of nonradiative recombination. The approach of using thick SQW with doped barriers remains a promising path towards low efficiency droop c-plane LEDs.

In this work, four InGaN/GaN SQW LEDs with different epitaxial structures were studied to examine the effects of QW width and doped barriers on the LED performance. The LEDs were grown by metalorganic chemical vapor deposition (MOCVD) on c-plane patterned sapphire substrates (PSS). The structures consisted of a 2 µm thick unintentionally doped (UID) GaN template layer, a 2 µm n-GaN layer, a 20-period n-$In_{0.04}Ga_{0.96}N$/GaN 2.2 nm/4.5 nm superlattice, a 30 nm n-GaN layer, a 12 nm UID GaN barrier or Si-doped n-GaN barrier ([Si] = 1.4×10^{19} cm^{-3}), a 3 nm or 9 nm undoped $In_{0.14}Ga_{0.86}N$ QW, a 2 nm UID GaN capping layer, a 10 nm or UID GaN barrier or Mg-doped p-GaN barrier([Mg] = 1.5×10^{19} cm^{-3}), a 26 nm p-$Al_{0.10}Ga_{0.90}N$ electron blocking layer (EBL), a 100 nm p-GaN, and a 10 nm p^+-GaN contact layer (Fig. 1(a)). The 3(9) nm SQW LEDs without and with the doped barriers are henceforth referred to as LED-3UD and LED-3D (LED-9UD and LED-9D), respectively. The intentional doping was calibrated via secondary ion mass spectroscopy (SIMS). The doping level of the barriers are lower than that of the LEDs in Ref. 12. Although this might lower the effectiveness in reducing F_{QW}, the lower doping helps to reduce the defect-related NRCs in the LEDs.

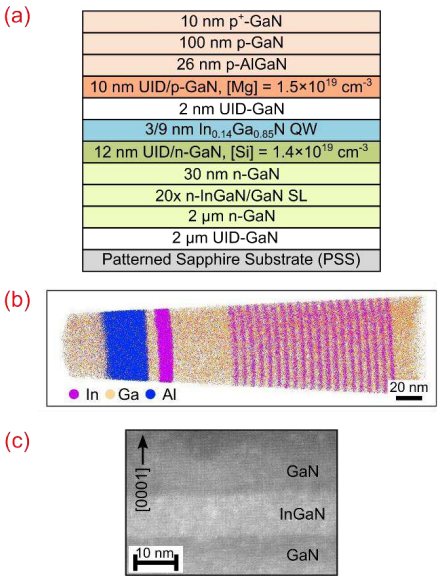

FIG. 1. (a) Schematic of the epitaxial structures. (b) Atom probe reconstruction and (c) HAADF-STEM image for LED-9D with a 9-nm-thick SQW.

Following the MOCVD growth, the indium composition and QW thickness were measured by x-ray diffraction (XRD) using a PANalytic MRD PRO diffractometer. Furthermore, the indium composition and thickness were also verified by atom probe tomography (APT) and high angle annular dark field scanning transmission electron microscopy (HAADF-STEM) respectively as shown in Figures 1(b)-1(c). The samples were then processed into LEDs. First, a 110 nm indium tin oxide (ITO) current spreading layer was deposited by electron-beam evaporation. Rectangular mesas (0.1 mm^2 active area) were then defined by reactive-ion etching the ITO and the epitaxial layers to reach the n-GaN layer. After that, a dielectric omnidirectional reflector (ODR) was deposited via ion beam deposition to serve as a reflective layer and a metal isolation layer. Common Al/Ni/Au n- and p-metal contacts were then deposited by electron-beam evaporation. After singulation, devices were mounted on silver headers, wire bonded, and encapsulated in silicone. The packaged devices were then tested in a calibrated integrating sphere at current densities up to 400 A/cm^2 under pulsed conditions (3-5% duty cycle with 10 μs pulse widths) to minimize heating. To study the F_{QW} in the QWs, biased photocurrent spectroscopy (BPCS) measurements were also carried out on all 4 LEDs.[18,19] The resulting photocurrent spectra are representative of optical absorption spectra assuming that the collection efficiency of photocurrent is independent of photon energy.[20] The bias dependence of the photocurrent spectra provides valuable information on the F_{QW} as it perturbs the absorption spectra at energies similar to the QW bandgap. In the BPCS setup, the LED was illuminated with monochromatic light using a TRIAX 180 monochromator with an Energetiq EQ-99 light source. The LED was biased with a Keithley 2400 sourcemeter. A 2 kΩ resistor was placed in series with the LED to allow the measurement of

the photocurrent through it. The additional voltage drop due to the resistor is negligible compared to the applied biases because of the small photocurrent. The optical beam was chopped at 82 Hz and the photocurrent signal was measured with a Princeton Applied Research 5209 lock-in amplifier. The photocurrent spectra were normalized to account for the wavelength dependence of the intensity of the light source. BPCS measurements were performed on the LEDs for applied biases varying from around +1 V to -2 V.

Figure 2(a) shows the photocurrent spectra for LED-3UD (3 nm QW, without doped barriers). A blueshift in the absorption edge has been observed as the applied bias changes from +1.2 V to -2 V (where negative sign indicates a reverse bias). In the conventional Ga-polar InGaN/GaN LEDs with p-side-up geometry, the polarization-related electric field (F_{pol}) in the QW is in the opposite direction of the *p-n* junction electric field (F_{pn}) in the diode. For most InGaN/GaN structures, since the F_{pol} is much larger than the F_{pn}, the net F_{QW} in the QW points towards the substrate. For LED-3UD, this remains true as confirmed by the simulations. By using a Schrödinger-Poisson drift-diffusion solver[21,22], the electric fields and band diagrams of the LEDs were simulated with 50% theoretical polarization values. Simulation parameters can be found in the Supplementary Material. As shown in Figure 2(c), at zero bias, the F_{QW} of LED-3UD is in the opposite direction of the F_{pn}. As a result, increasing the reverse bias leads to a reduction of the net F_{QW} and ultimately a blueshift in the absorption edge due to the reduced quantum confined Stark effect (QCSE). This trend is consistent with the BPCS results of *c*-plane InGaN/GaN MQW solar cells.[18] Excitonic features also appeared in the photocurrent spectra at applied biases of -1 V to -2 V. It is known that F_{QW} reduces the exciton binding energy.[23,24] The appearance of exciton peaks in the spectra indicates that the F_{QW} is close to zero at -1 V to -2 V biases.[17] From the simulations (Fig. 2(c)), the F_{QW} is indeed close to zero at a diode bias of -1 V. The slight discrepancy might be due to the uncertainty in the polarization values used in the simulations. A further increase in the reverse bias should invert the bands, leading to a redshift in the absorption edge. The redshift in the photocurrent spectra after -2 V (not shown) is difficult to observe due to the decreasing signal-to-noise ratio as a result of the increasing leakage current. LED-9UD demonstrated a similar trend (see Supplementary Material) except no excitonic features were observed. With a larger well width of 9 nm, the resultant lower exciton binding energy makes excitons unstable at room temperature.[24] The BPCS results verified that the F_{QW} of both LED-3UD and LED-9UD are in the opposite direction of the F_{pn} at zero bias. Consequently, with increasing forward bias, the F_{QW} continues to increase, exacerbating the QCSE, until the partial screening of the F_{pol} by injected free carriers happens at high current densities.

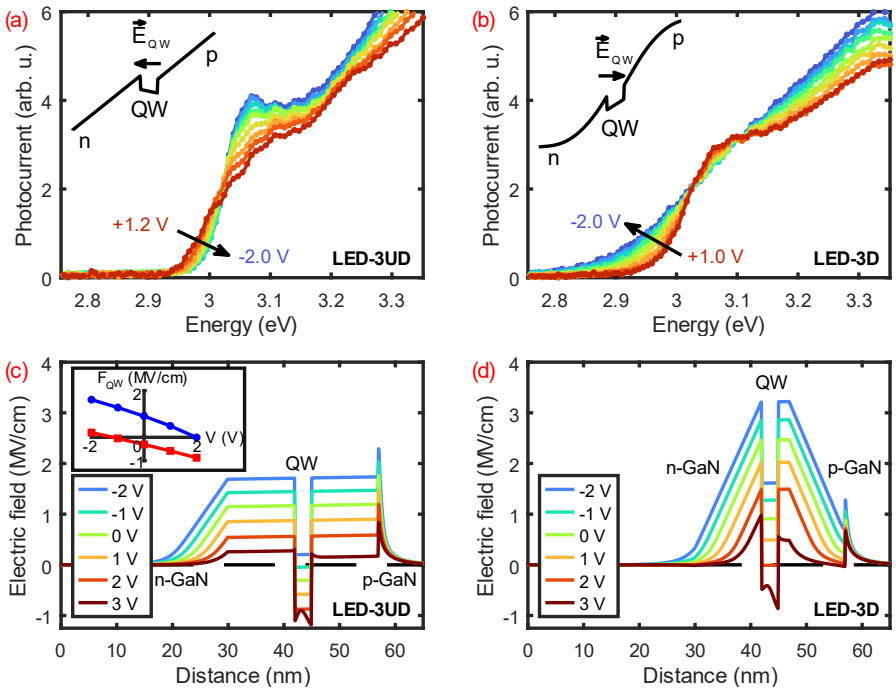

FIG. 2. Photocurrent spectra for (a) LED-3UD at -2 V to 1.2 V (0.4 V interval) and (b) LED-3D at -2 V to 0.8 V (0.4 interval) and at 1 V. Simulated electric fields for (c) LED-3UD and (d) LED-3D at different bias voltages. Positive electric fields point from the substrate towards the growth surface. The insets in (a) and (b) show the simulated conduction band diagrams at zero bias for LED-3UD and LED-3D, respectively. The inset in (c) shows the dependence of the internal electric field in the QW (F_{QW}) on bias voltages for LED-3UD (red) and LED-3D (blue).

Contrary to the results of LEDs without doped barriers (LED-3UD and LED-9UD), the absorption edges of photocurrent spectra for both LED-3D and LED-9D undergo a redshift as the applied bias varies from +1 V to -2 V. Only the photocurrent spectra for LED-3D (3 nm QW, with doped barriers) are shown in Figure 2(b) as the spectra for both LEDs are similar (spectra of LED-9D are given in Supplementary Material). Figure 2(d) shows the simulated electric fields of LED-3D under several biased conditions. These electric fields are useful to explain the opposite trends observed in BPCS between LEDs with and without the doped barriers. The thin UID region (5 nm and 11 nm for LED-3D and LED-9D respectively) combined with the highly doped barriers lead to an increase of the F_{pn} across the junction. At zero bias, the maximum F_{pn} is actually higher than the F_{pol} in the QW. Consequently, the net F_{QW} in the QW is in the same direction as the *p-n* junction field. As a result, the F_{QW} increases with the reverse bias, exacerbating the QCSE and thus causing the redshift in the absorption edge. The observed trends and simulations are in good agreement, verifying that the F_{QW} is indeed in the same direction of the F_{pn} at least in the BPCS applied bias

range of -2 V to +1 V (including zero bias). With increasing forward bias, the F_{QW} decreases and reaches zero at +2 V according to the simulations. However, this does not imply flat energy bands in the QW when the LEDs are turned on since further increase in forward bias results in non-zero F_{QW}. Furthermore, after device turn-on, the excess carriers in the QW also leads to a nonmonotonic electric field distribution inside the QW as shown in Figures 2(c) and 2(d) (+3 V).[25] Nonetheless, the F_{QW} in the LEDs with doped barriers are projected to be lower once the LEDs are in operating condition (>2.9 V) based on the trend of the BPCS results. The lower electric fields lead to flatter energy bands in the QW and an enhancement in the ground state electron-hole wavefunction overlap.

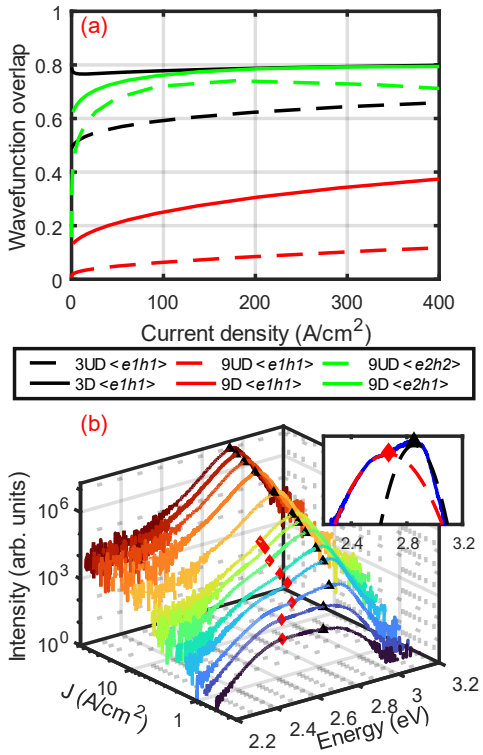

FIG. 3. (a) Simulated electron-hole wavefunction overlap as a function of current density of the 4 LEDs. (b) Electroluminescence spectra of LED-9UD at different current densities. The fitted ground state (diamond) and excited state (triangle) emission peaks are also shown in the figure. Inset: EL spectrum and the fitted curves (dashed lines) at 1 A/cm^2.

Figure 3(a) shows the simulated wavefunction overlap for the 4 LEDs as a function of current density, computed with the same Schrödinger-Poisson drift-diffusion solver mentioned above. Comparing the ground state <*e1h1*> overlap, it is clear that LEDs with doped barriers

exhibit a large overlap compared to their counterparts without doped barriers. However, the overlap of the thick QW LEDs is still small compared to that of thin QW LEDs which have a high degree of confinement. Therefore, for thick QW LEDs, transitions via excited states should also be considered as they can be efficient recombination paths due to the low <*e1h1*> transition rate.[26] The transitions with the highest overlap involving the first excited states for LED-9UD and LED-9D (<*e2h2*> and <*e2h1*> respectively) are shown in Figure 3(a). Other transitions are given in the Supplementary Material. Carriers in the excited states are less localized at the edges of the QW and have a larger spatial extent. Therefore, even with a thick QW, the overlap can be high and comparable to the <*e1h1*> overlap of thin QW LEDs. However, high wavefunction overlap by itself does not imply that the particular transition contributes significantly to the emission process as the radiative rate of each transition also depends on the population of the participating states.

To further investigate, the simulated energy band diagrams of LED-9UD and LED-9D at 50 A/cm^2 are presented in Figure 4(a). For LED-9UD, there are large electric fields near the edges of the QW where the ground states are confined. This leads to a sharp triangular profile at the n(p)-side of the valence (conduction) band, thereby causing a large energy separation between the eigenstates for both electrons and holes. On the other hand, for LED-9D which has a smaller F_{QW}, the regions at the edges of the QW are flatter, resulting in smaller energy separations. This can be easily understood using the simple case of infinite square well where the energy separation is inversely proportional to the well width. Here, the sharper triangle profile corresponds to a narrower well with increased confinement energy and separation between confined states. The observed trends still apply at different current densities as shown in Figures 4(b) and 4(c) where the computed eigenvalues of each eigenstate as a function of current density are plotted. For LED-9UD, in order to populate the excited states, the large energy difference between the ground states and excited states leads to a large population of carriers in the ground states. It is manifested in the measured electroluminescence (EL) spectra shown in Figure 3(b) which exhibited two peaks at a low current density, representing the ground state and the excited state emissions. The energy difference between the peaks is around 0.2 eV and is in good agreement with the calculated energy difference between <*e1h1*> and <*e2h2*> transitions (see Supplementary Material). With increasing current densities, the spectra are dominated by the excited state emission. On the other hand, given the small energy separation between the eigenstates for LED-9D, it is easier to populate the excited states without significant built-up of carriers in the ground states. Consequently, the EL spectra of LED-9D (see Supplementary Material) shows a single peak with a transition energy close to the more efficient <*e2h1*> transition. Therefore, it is clear that for both thick QW LEDs, transitions via excited states play a significant role in the emission process.

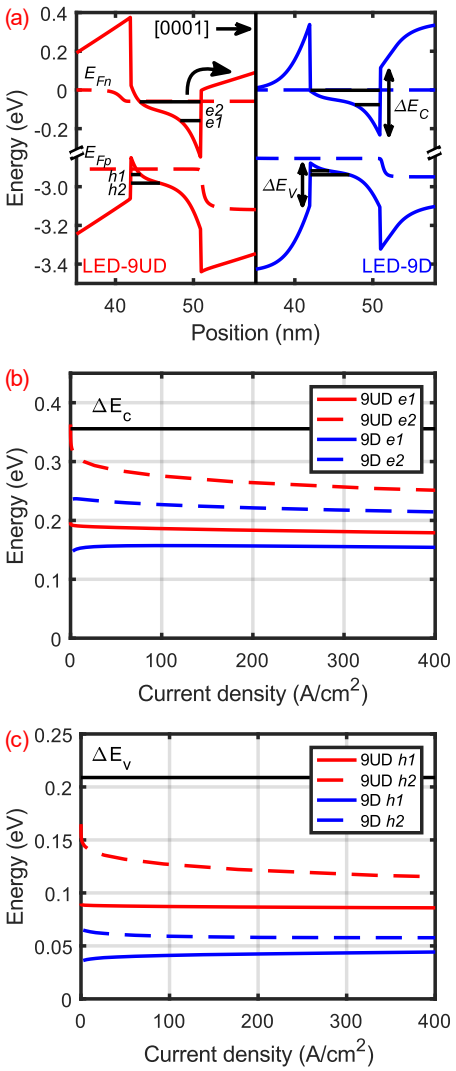

FIG. 4. (a) Band diagrams near the QWs of LED-9UD (red) and LED-9D (blue) at 50 A/cm^2. The energy levels of the eigenstates and the quasi-Fermi levels ($E_{Fn(p)}$) are also shown in the figures. (b) (c) The energy levels of the eigenstates relative to the bottom of the QW for electrons (b) and holes (c) as a function of current density. The conduction and valence band offsets (ΔE_C and ΔE_V) are also shown in the figures.

Compared to the ground states, the excited states are closer to the top of the well. Since the population in the excited states is important for both LED-9UD and LED-9D, carrier overflow from the QW via thermionic emission can be substantial for the lighter electrons. As shown in Figures 4(a) and (b), due to the large energy separation between eigenstates for LED-9UD, the excited state is close to the top of the well (p-side), resulting in a small effective barrier (measured relative to the first excited state). Compared to LED-9UD, there is a larger barrier for LED-9D due to the flatter band which brings down the energy levels of the excited states. In the p-side quantum barriers, the separation between the conduction band and the quasi-Fermi level of LED-9D is larger than that of LED-9UD, leading to less carrier overflow for LED-9D. On top of the lower excited states of LED-9D in the QW, the ionized acceptors in the doped barriers also pushes the quasi-Fermi level toward the valence band, thereby raising the conduction band, further improving the confinement of the electrons in the QW. Consequently, carrier overflow should impact LED-9UD more than LED-9D. The escaped electrons recombine swiftly once they reach the p-type region due to the short minority carrier lifetime. Even though there is a p-AlGaN EBL in the structure which aims to reduce carrier overflow, the defective AlGaN layer could also provide a pathway for trap-assisted Auger recombination (TAAR) which is a nonradiative recombination mechanism.[27,28] Therefore, LED-9UD is expected to have a lower external quantum efficiency (EQE) than LED-9D even though both LEDs have efficient recombination pathway via transitions involving excited states.

Figure 5(a) present the dependence of the EQE on the current density of the 4 LEDs. LED-3UD which is the most representative of commercial MQW LEDs has a peak EQE of 40% at 6 A/cm^2 with 43% efficiency droop at 400 A/cm^2. The efficiency droop is defined as: droop = (1 - EQE_J/EQE_{peak})×100%, where the EQE_{peak} and EQE_J represent the peak EQE and the EQE at different current densities, respectively. The significant droop observed in LED-3UD is common in *c*-plane InGaN/GaN LEDs where quantum efficiency typically peaks at current densities less than 10 A/cm^2 and drops substantially as current density increases.

With a thicker 9 nm QW, LED-9UD has a lower peak EQE (32%) than that of LED-3UD. The lower efficiency is likely due to the carrier overflow as previously discussed. However, at high current densities, where Auger recombination dominates, the EQE of LED-9UD surpasses that of LED-3UD due to the reduced carrier density resulting from the thicker QW. Similar efficiency trends have also been observed with increasing QW thickness in *c*-plane LEDs.[4,5]

With the doped barriers, LED-9D performed significantly better than LED-9UD, with the highest peak EQE (42%) among the 4 LEDs in the study. It has an EQE that peaks at 40 A/cm^2 and exhibits a low efficiency droop of 14% at 400 A/cm^2. Comparison of efficiency droop should only be made among LEDs with similar peak EQE. Therefore, only the efficiency droop of LED-3UD and LED-9D are reported. Although both LED-9UD and LED-9D have thick QWs, LED-9D has a much higher EQE at high current densities. Apart from the carrier overflow problem, LED-9UD also has a large ground state population due to the much lower $\langle e1h1 \rangle$ transition rate and large energy separation between ground and excited states. This partially negates the benefit of using thicker QWs which are aimed at reducing carrier densities. Therefore, doped barriers, which helps lowering F_{QW}, are essential in achieving efficient thick QW LEDs with low droop.

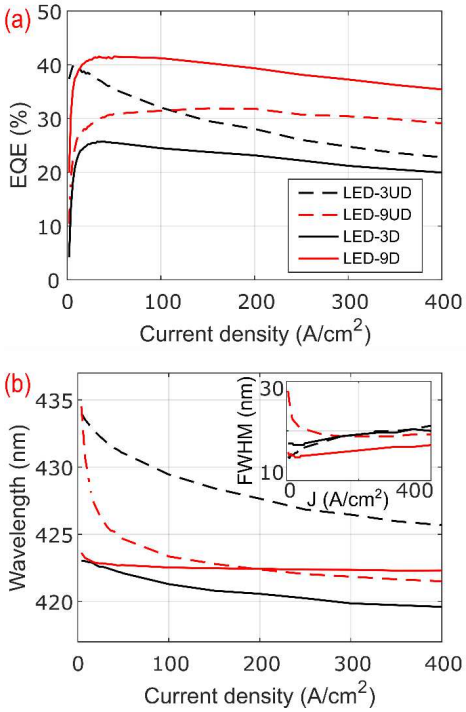

FIG. 5. (a) External quantum efficiency and (b) EL peak wavelength versus current density of the 4 LEDs. Inset: Full width at half maximum (FWHM) versus current density.

On the other hand, LED-3D has the lowest EQE in the study regardless of the injected current densities. The reduced F_{QW} in the QW due to the doped barriers does not benefit LED-3D as much as LED-9D. This is because thin QW LEDs without doped barriers already have an apparently sufficient wavefunction overlap due to the thin confinement region. Conversely, these doped barriers potentially introduce defect-related NRCs, resulting in a higher SRH rate which explains the low efficiency of LED-3D.[12] In contrast, its thick QW counterpart (LED-9D) is not significantly impacted by the increased NRCs from the doped barriers. It was suggested that SRH recombination takes place close to the middle of the QW, where the overlap of the e-h wavefunctions is maximum and not at the defective QW/barrier interfaces.[29] For LED-9D with a thicker QW, the distance between the SRH recombination plane, which is possibly in middle of the QW, and the NRCs in the doped barriers is larger. This might be a possible explanation for the high quantum efficiency of LED-9D, even at low current densities where SRH recombination dominates.

Figure 5(b) shows the EL peak wavelengths of the LEDs as a function of current density. The peak wavelengths of LED-3UD and LED-9UD exhibit blueshifts of 8 nm and 13 nm, respectively, over the measured range (1-400 A/cm^2). The blueshifts with increasing current density are common in *c*-plane LEDs, and can be explained by the reduction of QCSE due to free carrier screening of F_{pol}.[30,31] On the other hand, a reduced wavelength shift of 3 nm and 1 nm is observed for the LEDs with doped barriers (LED-3D and LED-9D respectively). Similar small wavelength shifts were also reported for nonpolar and semipolar LEDs where F_{pol} is absent or largely reduced.[6,7,32] The excellent wavelength stability with respect to current density is a desirable feature for display applications.[33] Both LEDs with doped barriers also have shorter emission wavelengths for different reasons. For LED-3D, it is due to the smaller F_{QW} induced redshift, whereas for LED-9D, the shorter emission wavelengths are a result of the higher energy transitions involving excited states. The full width at half maximum (FWHM) of the LEDs (inset of Fig. 5(b)) does not vary much with increasing current densities except for LED-9UD which has a larger FWHM at low current densities due to the contribution of both ground state and excited state emissions.

In summary, we have demonstrated *c*-plane InGaN/GaN LEDs with low efficiency droop using a thick SQW with doped barriers. Through biased photocurrent spectroscopy, we showed that the F_{QW} of the LEDs with doped barriers is in the same direction as the F_{pn} at zero bias, implying smaller F_{QW} in the QWs when LEDs are in operating conditions. Even with the improvement of ground state wavefunction overlap, thick QW LEDs strongly rely on excited state transitions as observed spectroscopically. Without doped barriers, thick QW LED suffers from carrier overflow due to the poor confinement of carriers in the excited states. On the other hand, with doped barriers, the F_{QW} is reduced, resulting in a flatter band and better confinement of such carriers in the QW, diminishing carrier overflow. Properly designed doped barriers are essential in achieving low droop and efficient thick InGaN/GaN SQW LEDs.

SUPPLMENTARY MATERIAL

See supplementary material for more experimental results (BPCS, EL spectra, J-V curve) and simulation results (wavefunction overlap, transition energy, and parameters used).

ACKNOWLEGMENTS

This work was supported by the Solid State Lighting and Energy Electronics Center (SSLEEC), the Simons Foundation (Grant Nos. 601952, J.S.S. and 601954 C.W.), the National Science Foundation (NSF) RAISE program (Grant No. DMS-1839077), the U.S. Department of Energy under Award No. DE-EE0008204, Sandia National Laboratories (Award No. 2150283), and UCSB-Collaborative Research in Engineering, Science and Technology (CREST). A portion of this work was performed in the UCSB Nanofabrication Facility, an open access laboratory. The authors would like to thank Dr. Yuh-Renn Wu, Wan Ying Ho, and Kai Shek Qwah for helpful discussions.

CONFLICT OF INTEREST

The authors have no conflicts to disclose.

DATA AVAILABILITY

The data that support the findings of this study are available from the corresponding author upon reasonable request.

References

[1] J. Cho, E.F. Schubert, and J.K. Kim, Laser & Photonics Rev. **7**, 408 (2013).

[2] J.-I. Shim, in *III-Nitride Based Light Emitting Diodes and Applications.*, edited by T.-Y. Seong, J. Han, H. Amano, and H. Morkoç (Springer Netherlands, Dordrecht, 2013), pp. 153–195.

[3] C. Weisbuch, M. Piccardo, L. Martinelli, J. Iveland, J. Peretti, and J.S. Speck, Phys. Status Solidi **212**, 899 (2015).

[4] N.F. Gardner, G.O. Müller, Y.C. Shen, G. Chen, S. Watanabe, W. Götz, and M.R. Krames, Appl. Phys. Lett. **91**, 243506 (2007).

[5] V. Avrutin, S. din A. Hafiz, F. Zhang, Ü. Özgür, H. Morkoç, and A. Matulionis, J. Vac. Sci. & Technol. A **31**, 50809 (2013).

[6] D.L. Becerra, Y. Zhao, S.H. Oh, C.D. Pynn, K. Fujito, S.P. DenBaars, and S. Nakamura, Appl. Phys. Lett. **105**, 171106 (2014).

[7] S.H. Oh, B.P. Yonkee, M. Cantore, R.M. Farrell, J.S. Speck, S. Nakamura, and S.P. DenBaars, Appl. Phys. Express **9**, 102102 (2016).

[8] C.S. Xia, Z.M. Simon Li, Z.Q. Li, Y. Sheng, Z.H. Zhang, W. Lu, and L.W. Cheng, Appl. Phys. Lett. **100**, 263504 (2012).

[9] A. David, M.J. Grundmann, J.F. Kaeding, N.F. Gardner, T.G. Mihopoulos, and M.R. Krames, Appl. Phys. Lett. **92**, 53502 (2008).

[10] M. Peter, A. Laubsch, W. Bergbauer, T. Meyer, M. Sabathil, J. Baur, and B. Hahn, Phys. Status Solidi **206**, 1125 (2009).

[11] V. Fiorentini, F. Bernardini, F. Della Sala, A. Di Carlo, and P. Lugli, Phys. Rev. B **60**, 8849 (1999).

[12] N.G. Young, R.M. Farrell, S. Oh, M. Cantore, F. Wu, S. Nakamura, S.P. DenBaars, C. Weisbuch, and J.S. Speck, Appl. Phys. Lett. **108**, 61105 (2016).

[13] T. Deguchi, A. Shikanai, K. Torii, T. Sota, S. Chichibu, and S. Nakamura, Appl. Phys. Lett. **72**, 3329 (1998).

[14] G. Franssen, T. Suski, P. Perlin, R. Bohdan, A. Bercha, W. Trzeciakowski, I. Makarowa, P. Prystawko, M. Leszczyński, I. Grzegory, S. Porowski, and S. Kokenyesi, Appl. Phys. Lett. **87**, 41109 (2005).

[15] E. Kioupakis, Q. Yan, and C.G. de Walle, Appl. Phys. Lett. **101**, 231107 (2012).

[16] A. David, N.G. Young, C. Lund, and M.D. Craven, Appl. Phys. Lett. **115**, 193502 (2019).

[17] A. David and M.J. Grundmann, Appl. Phys. Lett. **97**, 33501 (2010).

[18] M. Piccardo, C.-K. Li, Y.-R. Wu, J.S. Speck, B. Bonef, R.M. Farrell, M. Filoche, L. Martinelli, J. Peretti, and C. Weisbuch, Phys. Rev. B **95**, 144205 (2017).

[19] R.T. Collins, K. v. Klitzing, and K. Ploog, Phys. Rev. B **33**, 4378 (1986).

[20] H. Helmers, C. Karcher, and A.W. Bett, Appl. Phys. Lett. **103**, 32108 (2013).

[21] See http://yrwu-wk.ee.ntu.edu.tw/ for more information on the Schrödinger-Poisson drift-diffusion solver developed by Y.-R. Wu *et al*..

[22] C.-K. Li, M. Piccardo, L.-S. Lu, S. Mayboroda, L. Martinelli, J. Peretti, J.S. Speck, C. Weisbuch, M. Filoche, and Y.-R. Wu, Phys. Rev. B **95**, 144206 (2017).

[23] R. Cingolani, A. Botchkarev, H. Tang, H. Morkoç, G. Traetta, G. Coli, M. Lomascolo, A. Di Carlo, F. Della Sala, and P. Lugli, Phys. Rev. B **61**, 2711 (2000).

[24] S.-H. Park, J.-J. Kim, and H.-M. Kim, J. Korean Phys. Soc. **45**, 582 (2004).

[25] S.Y. Karpov, in *Nitride Semicond. Devices Princ. Simul.*, edited by J. Piprek (Wiley-VCH, Weinheim, 2007), pp. 303–325.

[26] G. Muziol, H. Turski, M. Siekacz, K. Szkudlarek, L. Janicki, M. Baranowski, S. Zolud, R. Kudrawiec, T. Suski, and C. Skierbiszewski, ACS Photonics **6**, 1963 (2019).

[27] D.J. Myers, K. Gelžinytė, A.I. Alhassan, L. Martinelli, J. Peretti, S. Nakamura, C. Weisbuch, and J.S. Speck, Phys. Rev. B **100**, 125303 (2019).

[28] T.A. Henry, A. Armstrong, A.A. Allerman, and M.H. Crawford, Appl. Phys. Lett. **100**, 43509 (2012).

[29] A. David, C.A. Hurni, N.G. Young, and M.D. Craven, Appl. Phys. Lett. **111**, 233501 (2017).

[30] T. Takeuchi, S. Sota, M. Katsuragawa, M. Komori, H. Takeuchi, H. Amano, and I. Akasaki, Jpn. J. Appl. Phys. **36**, L382 (1997).

[31] S. Chichibu, T. Sota, K. Wada, and S. Nakamura, J. Vac. Sci. & Technol. B Microelectron. Nanom. Struct. Process. Meas. Phenom. **16**, 2204 (1998).

[32] Y.-D. Lin, A. Chakraborty, S. Brinkley, H.C. Kuo, T. Melo, K. Fujito, J.S. Speck, S.P. DenBaars, and S. Nakamura, Appl. Phys. Lett. **94**, 261108 (2009).

[33] R. Lu, Q. Hong, Z. Ge, and S.-T. Wu, Opt. Express **14**, 6243 (2006).

(a)

10 nm p^+-GaN
100 nm p-GaN
26 nm p-AlGaN
10 nm UID/p-GaN, [Mg] = 1.5×10^{19} cm^{-3}
2 nm UID-GaN
3/9 nm $In_{0.14}Ga_{0.85}N$ QW
12 nm UID/n-GaN, [Si] = 1.4×10^{19} cm^{-3}
30 nm n-GaN
20x n-InGaN/GaN SL
2 µm n-GaN
2 µm UID-GaN
Patterned Sapphire Substrate (PSS)

(b)

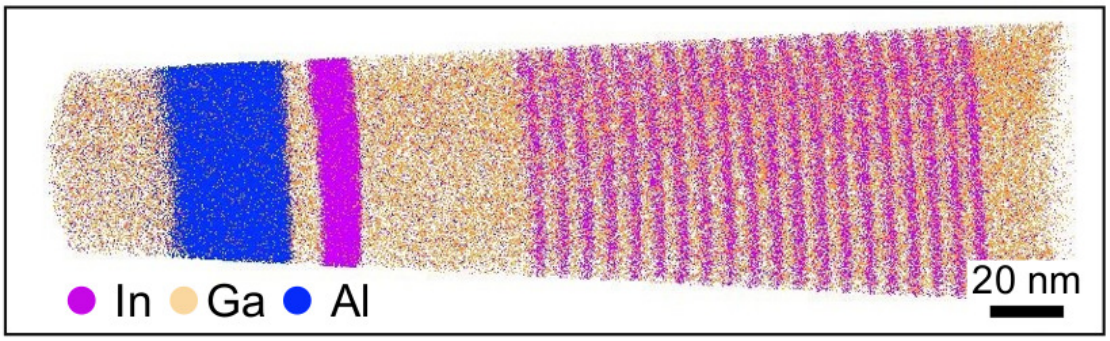

(c)

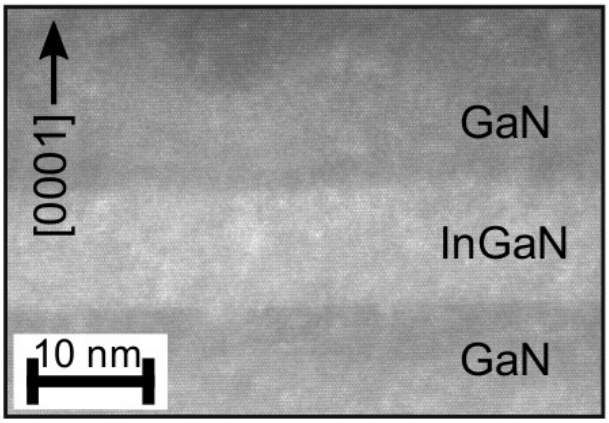

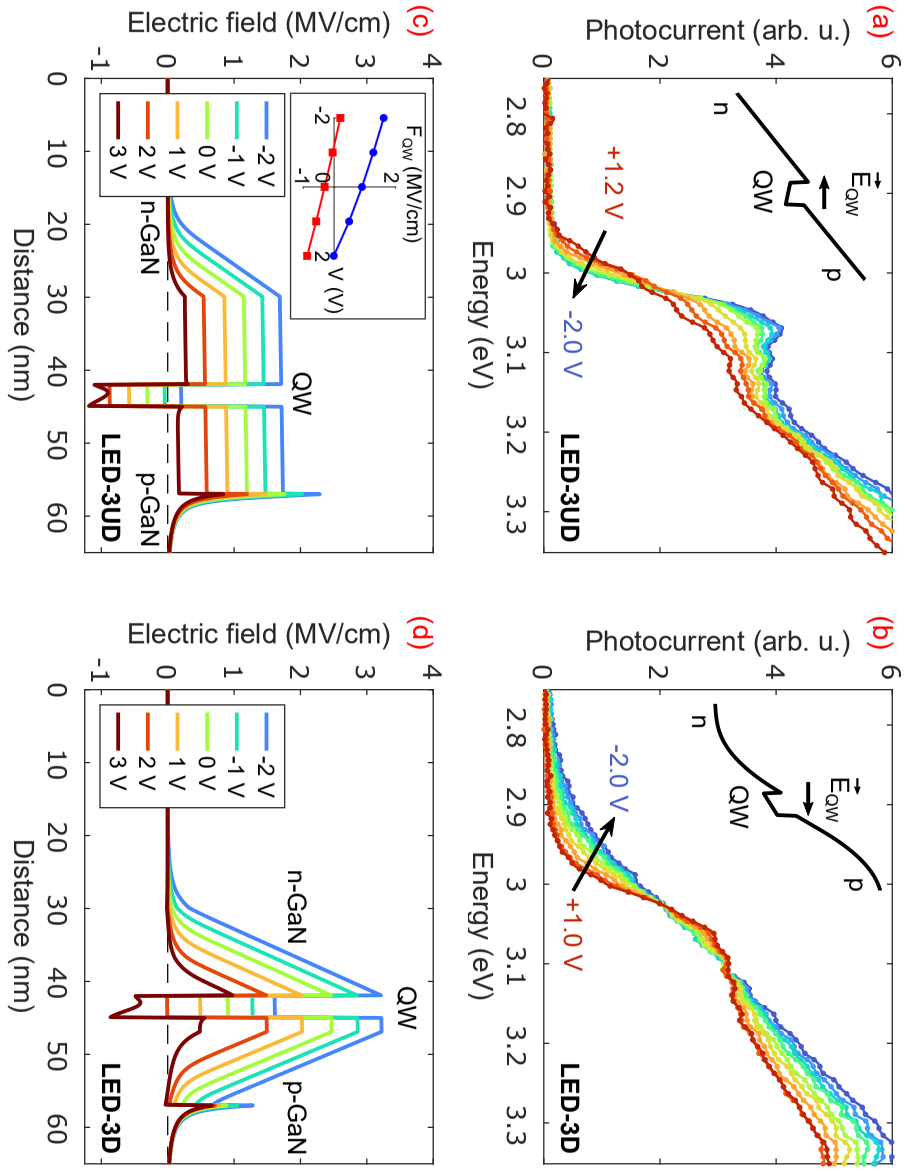

Applied Physics Letters

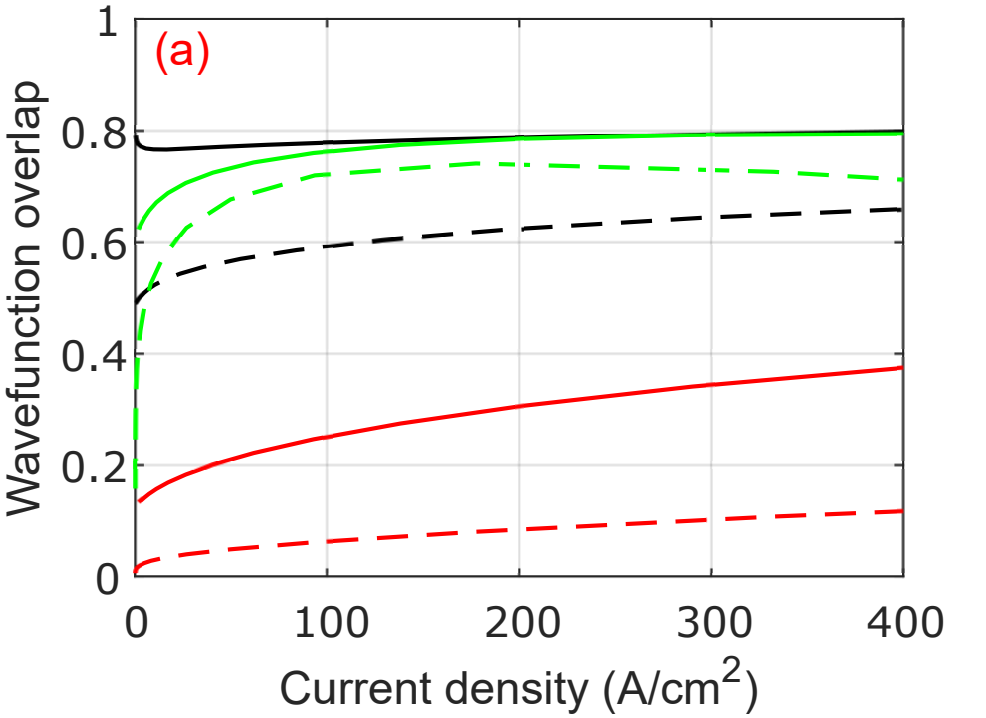

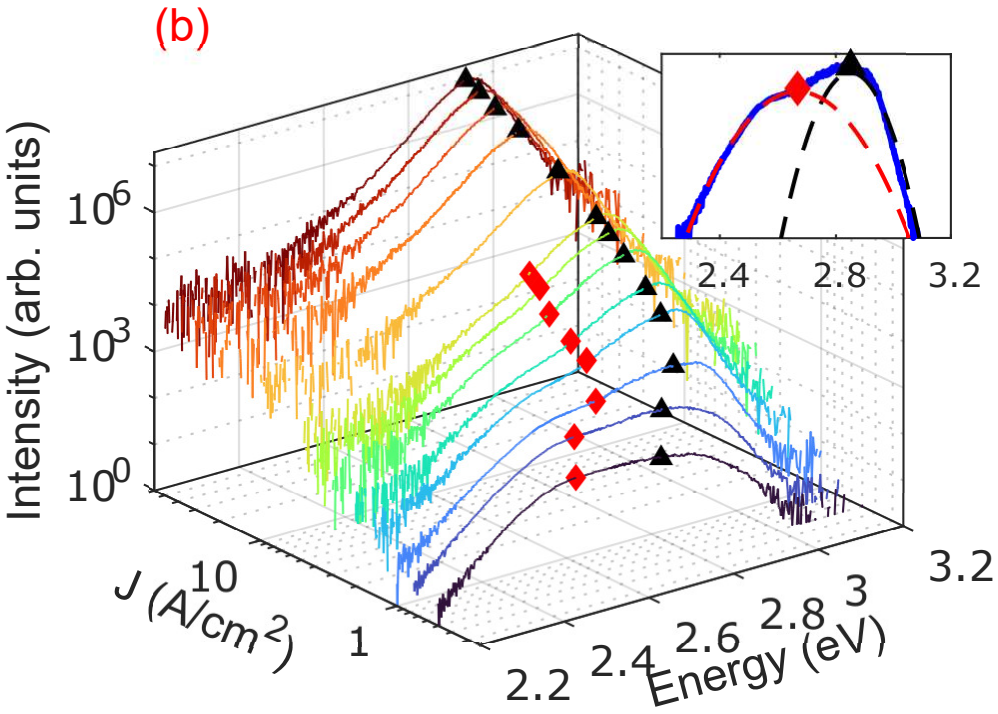

AIP Publishing